# Automated sorting of live *C. elegans* using laFACS

**To the Editor:** A recent paper in *Nature Methods* describes the use of fluorescence-activated cell sorting (FACS) to sort *Caenorhabditis elegans* embryos[1]. Here we report a FACS-based method to sort live *C. elegans* larvae, which permits us to rapidly collect large quantities of live genotyped worms from a mixed population. Using *GFP*-marked balancer chromosomes (**Fig. 1a**) and live-animal FACS (laFACS), we routinely collected >100,000 genotyped worms in less than one hour. To test laFACS, we combined it with large-scale RNA interference (RNAi) screening and identified genetic interactors of *mel-28*, an important regulator of nuclear envelope and chromatin functions[2–5].

Although a FACS machine is designed to sort single cells, a few modifications enabled us to sort ~0.25-mm-long L1 *C. elegans*. First, we used a reduced drop-drive frequency of ~16.4 kHz to not damage the larvae. We also used a 100-µm nozzle and set a gate to capture events with a high forward-scatter signal (**Fig. 1b**), confining our collections to larger objects (**Supplementary Methods**). After worm sorting, the same FACS machine could be used for several other applications, including sorting of yeast, *Drosophila melanogaster* cells, mammalian cells and plant protoplasts. The worm sort had no impact on these applications, and the worm-specific FACS machine modifications were easily reversed to accommodate single-cell applications.

We used laFACS to collect *mel-28* homozygous worms from a mixed population. *mel-28* homozygous hermaphrodites derived from heterozygous mothers appear phenotypically indistinguishable from wild-type worms but produce only inviable progeny. This selection is usually performed manually and thus is not amenable to large-scale applications. We first generated a *GFP*-marked strain in which the *mel-28(t1684)* mutation is balanced over a chromosome bearing *lag-2::GFP*[6] (**Fig. 1a**). We sorted L1 worms, collecting GFP-negative *mel-28(t1684)* homozygotes. We selected GFP-negative larvae on the basis of the ratio of green (GFP fluorescence; 530/30 nm) to red (red-spectrum autofluorescence; 610/20 nm) signal (**Fig. 1c,d**). We separated GFP-positive and GFP-negative worms (**Supplementary Fig. 1**). Typically, from a population of 600,000 larvae, we retrieved ~130,000 healthy worms after one sort. This first-pass population was ~95–98% homozygous ($n > 1{,}000$, verified by microscopy). A second sort recovered an essentially 100% pure population of about 100,000 homozygous larvae ($n > 20{,}000$, verified by microscopy and genetic analysis). This scheme can be easily adapted for the majority of *C. elegans* genes using available balancers.

We used the collected homozygous *mel-28* worms to perform an RNAi-based synthetic interaction screen using clones representing chromosome 1 genes[7]. The ability to easily collect large amounts of *mel-28* homozygous worms allowed us to perform the RNAi analysis repeatedly (up to 16 times). From over 2,000 genes tested, 12 showed synthetic phenotypes with *mel-28*: *npp-2, npp-4, npp-12, npp-14, npp-17, his-67, his-68, exos-3, pas-5, phi-56, rpa-0 and rpl-30* (**Supplementary Fig. 2** and **Supplementary Table 1**). These results agreed well with *mel-28*'s role in coordinating chromatin and nuclear envelope functions[2,3]. Obtaining large quantities of pure mutant populations could also be useful for chemical screens, microarrays or biochemical assays, expanding the arsenal of high-throughput tools available in *C. elegans*.

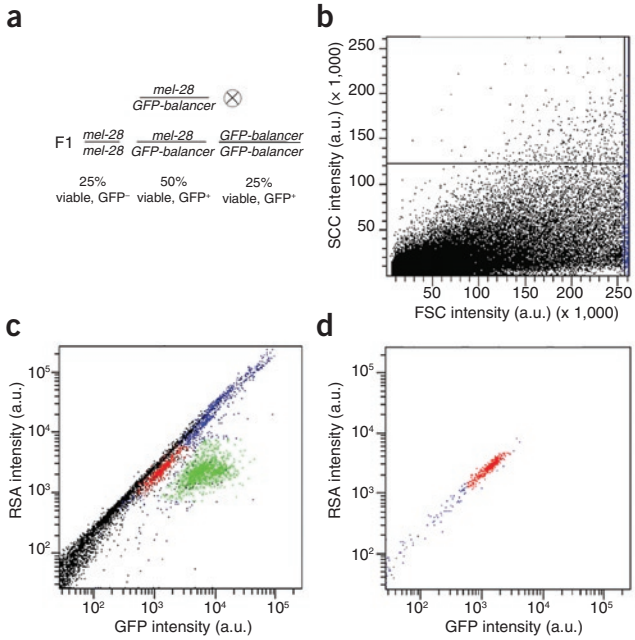


**Figure 1** | laFACS of GFP-negative L1 larvae. (**a**) Genetic scheme. A *mel-28* mutant allele is kept over a balancer chromosome containing a *GFP* marker and a recessive lethal allele. GFP-negative progeny (F1) are *mel-28* homozygotes and grow up to produce only dead embryos. (**b**) A dot-plot of forward scatter (FSC) versus side scatter (SSC) signals. The gate on FSC separates the larvae (blue) from debris (black). (**c**) A dot plot of red-spectrum autofluorescence (RSA) versus GFP signals. GFP-positive *mel-28* heterozygotes (green) are defined and used to gate for the GFP-negative larvae (red) to be sorted. (**d**) A dot plot of the RSA versus GFP signals after the sort.

*Note: Supplementary information is available on the Nature Methods website.*

**ACKNOWLEDGMENTS**

This work was partly funded by the US National Institute of Child Health and Human Development (R01HD046236) and the National Human Genome Research Institute (U01 HG004276) to F.P., the National Institutes of Health (R01GM078279-01) to K.D.B. and by the National Science Foundation (0827858) to A.G.F. Nematode strains were provided by the *Caenorhabditis* Genetics Center, which is funded by the National Institutes of Health National Center for Research Resources.

**COMPETING FINANCIAL INTERESTS**

The authors declare no competing financial interests.

**Anita G Fernandez[1,2], Emily K Mis[1], Bastiaan O R Bargmann[1], Kenneth D Birnbaum[1] & Fabio Piano[1]**

[1]Department of Biology and Center for Genomics and Systems Biology, New York University, New York, New York, USA. [2]Department of Biology, Fairfield University, Fairfield, Connecticut, USA.
e-mail: afernandez@fairfield.edu

PUBLISHED ONLINE 2 MAY 2010; DOI:10.1038/NMETH.F.304


1. Stoeckius, M. *et al. Nat. Methods* **6**, 745–751 (2009).
2. Fernandez, A.G. & Piano, F. *Curr. Biol.* **16**, 1757–1763 (2006).
3. Galy, V., Askjaer, P., Franz, C., Lopez-Iglesias, C. & Mattaj, I.W. *Curr. Biol.* **16**, 1748–1756 (2006).
4. Rasala, B.A., Orjalo, A.V., Shen, Z., Briggs, S. & Forbes, D.J. *Proc. Natl. Acad. Sci. USA* **103**, 17801–17806 (2006).
5. Franz, C. *et al. EMBO Rep.* **8**, 165–172 (2007).
6. Edgley, M.K., Baillie, D.L., Riddle, D.L. & Rose, A.M. in *WormBook* (The *C. elegans* research community, 2006).
7. Kamath, R.S. *et al. Nature* **421**, 231–237 (2003).


## Software for bead-based registration of selective plane illumination microscopy data

**To the Editor:** Selective plane illumination microscopy (SPIM)[1] allows isotropic, time-lapse, *in toto* imaging of large, living biological specimens by acquiring three-dimensional (3D) images of the same sample from multiple angles (views). However, to realize the potential of multiview SPIM imaging, it is necessary to reconstruct a single 3D image from the individual views[2] (**Fig. 1a**, **Supplementary Fig. 1** and **Supplementary Video 1**).

SPIM multiview registration is complicated by degradation of the signal along the illumination as well as detection axes (**Fig. 1b**), limited overlap between the views, different orientations of the optical sections and development of the specimen during acquisition. We developed a SPIM registration method and implemented it in a plugin for Fiji. The software enables efficient, sample-independent registration of multiview SPIM acquisitions using fluorescent beads in rigid mounting medium as fiduciary markers.

We first detected the beads with subpixel accuracy using a difference of Gaussian[3] filter, reducing the registration problem to the matching of point clouds. To efficiently identify corresponding beads in different views, we developed a translation and rotation invariant local geometric descriptor (**Fig. 1c**) that identifies each bead by the unique constellation of its neighboring beads. This constellation is preserved across views transformed by rotation and translation in three dimensions. For efficient matching, we defined an orthogonal local coordinate system (**Supplementary Fig. 2**) in each descriptor, expressing the 3D constellation of four beads by a vector of six scalar values, achieving translation and rotation invariance. Similar descriptors in different views have a small Euclidean distance in the six-dimensional descriptor space, and for efficient identification of nearest neighbors we presorted the six-dimensional scalar vectors using a hierarchical tree-based algorithm to reduce the matching problem to logarithmic complexity. Constellations of four beads that accidentally look similar (false correspondences) are rejected using the random sample consensus[4] on an affine transformation model followed by a robust regression filter (**Supplementary Methods**).

In the final step of the registration framework, we globally minimized the displacement of all true correspondences identified in all pairs of views using an iterative optimization scheme resulting in an affine transformation model for each view (**Fig. 1d**, **Supplementary Fig. 3** and **Supplementary Videos 2** and **3**). Typically, we identified thousands of corresponding bead descriptors equally distributed around the imaged sample, and the global optimization converged within seconds to a final average displacement of about one pixel

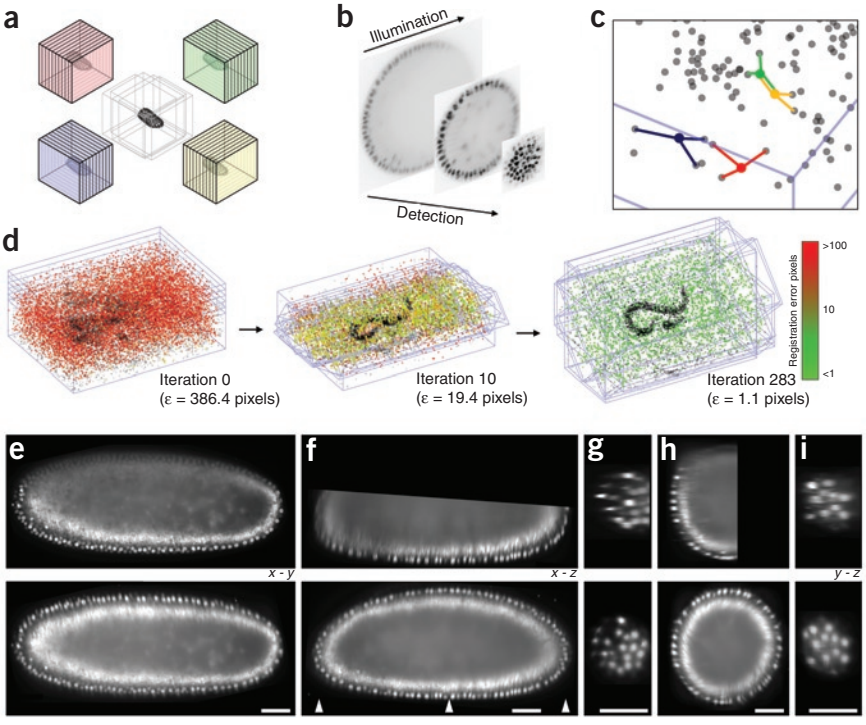


**Figure 1** | Bead-based registration framework. (**a**) Several stacks of two-dimensional images of the same specimen acquired from different views have to be registered to obtain a single 3D image. (**b**) Three SPIM sections of *Drosophila* embryo stained with nuclear marker show the deterioration of the fluorescence signal along the illumination and detection axes. (**c**) Four color-coded examples of 3D constellations of four beads (central bead and its three nearest neighbors forming a bead descriptor) used to identify corresponding beads in different views (blue lines show view boundary in three dimensions, and gray circles represent the beads). (**d**) A 3D visualization of the global optimization progress on eight SPIM views of fixed *Caenorhabditis elegans* worm. Displacement of corresponding bead descriptors is color-coded from red (maximum displacement) to green (minimal displacement). The global optimization is initialized with all views on top of each other. Three iterations (0, 10 and 283) are shown along with average displacement across all descriptors. (**e**–**i**) Sections through living *Drosophila* embryo expressing His-YFP in all cells; imaged and reconstructed from seven SPIM views (bottom) compared to single SPIM view (top). Single-view acquisitions were stopped approximately in the middle of the embryo to avoid optical aberrations resulting from light scattering and to speed up the acquisition. The lateral resolution in the reconstructed multiview image (**e**) is comparable with the axial resolution (**f**) and is superior to the resolution of the single view. *y*-*z* sections (**g**–**i**) at positions marked by white arrowheads in **f**. Scale bars, 50 μm.